Journal of Applied Polymer Science

# Investigation of polybenzoxazine gelation using laser light scattering

**Hui Li,[1] Senlong Gu,[2] Shantel Thomas,[3] Tianbo Liu,[1] Sadhan C. Jana [2]**

[1]Department of Polymer Science, University of Akron, Akron, Ohio 44325
[2]Department of Polymer Engineering, University of Akron, Akron, Ohio 44325
[3]Department of Chemistry and Biochemistry, McMurry University, Abilene, Texas 79697
H. Li and S. Gu contributed equally to this article.
Correspondence to: S. C. Jana (E-mail: janas@uakron.edu)

**ABSTRACT:** The mechanism of phase growth and gelation due to polymerization of benzoxazine into polybenzoxazine (PBZ) in dimethylsulfoxide and *N*-methyl-2-pyrrolidone was monitored using laser light scattering. The radius of gyration ($R_g$) and hydrodynamic radius ($R_h$) increased gradually with time, confirming nucleation and growth as the mechanism of polymerization-induced phase separation of PBZ in both the solvents. The experimental data inferred from laser light scattering and scanning electron microscopy established that the PBZ gel networks were formed by spherical building blocks in dimethylsulfoxide and by cylindrical strands in *N*-methyl-2-pyrrolidone. In the latter case, the cylindrical strands originated from joining of several spheres. © 2017 Wiley Periodicals, Inc. J. Appl. Polym. Sci. **2018**, *135*, 45709.

**KEYWORDS:** gels; kinetics; morphology; nanostructured polymers

Received 29 June 2017; accepted 16 August 2017
**DOI: 10.1002/app.45709**

## INTRODUCTION

Mesoporous materials received tremendous attention in the last two decades due to their widespread applications in gas storage,[1] chemical separation,[2] and catalysis.[3] Aerogels are a class of mesoporous solid materials formed by nanometer-sized solid networks filled with high percentage of air.[4,5] They offer a set of interesting properties such as, low thermal conductivity,[6] high specific surface area,[7] and low bulk density.[8] Aerogels are generally obtained from precursor gels by replacing the liquid with air in a supercritical drying step. The supercritical drying process leaves interconnected voids without structural collapse which are viewed as the pores in aerogels. These pores show diversity in geometry depending upon the nature of the solid building blocks, the amount of solids in the precursor gels, and the mechanism of polymerization induced phase separation.[9–14] The diameter of the pores range from 1 nm to a few micrometer.

Recently, Gu *et al.*[9] reported the dependence of the shape and size of solid networks in polybenzoxazine (PBZ) aerogels on the nature of the solvents and reaction temperature in the gelation step. The mesoporous PBZ aerogels prepared with the same solid content showed different building blocks, for example, spheres in dimethylsulfoxide (DMSO) and cylindrical strands in *N*-methyl-2-pyrrolidone (NMP) which in turn produced different Brunauer–Emmett–Teller surface area, pore size distribution, and pore volume. For example, the aerogels from the gels prepared at 130 °C in DMSO and NMP provided Brunauer–Emmett–Teller surface area of 92 and 82 $m^2/g$ and bulk density of 0.45 and 0.37 $g/cm^3$. The pore size distribution was broad in the case of materials prepared in NMP while it was narrow with mean diameter ~20 nm for materials prepared in DMSO. Such a difference in pore architecture of gels may be beneficial in the design of drug delivery systems, catalysts, and air filters. Liu reported silica aerogels with fibrous and globular networks[15] formed in different stages of spinodal decomposition. The spheres formed in the early stage while the strands formed in the later stage due to structural coarsening. Leventis *et al.*[10] observed that the morphology of polyurea aerogels changed from a regime of collections of strands to a regime with aggregation of spheres due to an increase of the concentration of the monomer. These authors attributed the formation of two types of polyurea networks to polymerization induced nucleation and growth. However, no direct evidence is presented in current literature on the growth of the gel networks starting with nucleation. In this work, we introduced laser light scattering (LLS) technology to dynamically characterize the gelation process and to understand the mechanism of growth of two different building blocks in PBZ gels produced in NMP and DMSO.

Additional Supporting Information may be found in the online version of this article.

LLS, including static light scattering (SLS) and dynamic light scattering (DLS), is often used to study polymers and nanoparticles in dilute solutions.[16–19] SLS measures the total scattered intensity from the solution which can lead to information on radius of gyration ($R_g$) and weight-average molecular weight of the particles. The scattered intensity can be regarded as an indicator of the gelation process based on Rayleigh-Gans-Debye equation,[16,20] where the scattered intensity increases as the number and the size of the scattering site increase. The magnitude of intensity is, however, more sensitive to the size variation.[16,20] On the other hand, DLS data provide hydrodynamic radius ($R_h$) values with the assistance of CONTIN[20] analysis. The combination of $R_h$ and $R_g$ values can help in the understanding of the geometry of the particles in solutions. In this work, we determined the size and the shape of PBZ nanoparticles at different elapsed times during gelation in solvents NMP and DMSO.

## EXPERIMENTAL

In a typical experiment, 1.100 g of benzoxazine (BZ) and 0.011 g of *p*-toluenesulfonic acid (TSA) were dissolved in 4.0 mL pure solvent (DMSO or NMP). The filtered solution was kept in an oil bath at 120 °C in order to initiate and continue the cationic polymerization process[21] (Figure 1) until the solution turned into a gel. Specimens were taken out of the reaction system at prescribed time intervals, diluted with fresh solvent, and were examined by LLS method to record the structural information of the polymer domains until the gel point was reached. Each time, a 5.0 μL hot solution taken out of the reaction system was added into 2.0 mL filtered solvent (DMSO or NMP) to reach a final concentration of 0.68 mg/mL. The solutions were then cooled down to room temperature and the data were taken by LLS method. It should be noted that dilute solutions were used in LLS study to ensure the accuracy of the results. The LLS tests were conducted at room temperature due to the requirement of the instrument. We assumed the following: (1) the reaction mass was homogeneous, (2) polymerization of PBZ was terminated due to dilution with the solvent and lowering of the temperature to room temperature, and (3) the polymer domains did not undergo swelling and their morphologies did not change much before the data were taken by LLS method.

## RESULTS AND DISCUSSION

Figure 2(a,b) shows the plots of scattered intensities ($I$) versus time obtained from SLS measurements. In both solvents, at the very beginning of polymerization, the values of $I$ are close to zero as only the small BZ monomer molecules were present in the solution. With the progress of polymerization, the intensity increased slowly (Stage I) followed by a rapid growth (Stage II). Specifically, in Stage I, the monomers participated in initiation reactions with $H^+$, formed the propagation centers, and produced the oligomers.[22] Although the number of oligomers increased in this stage, no obvious increase of scattered intensity was observed indicating that the increase in the size of the oligomers was limited. In contrast, the scattered intensity increased dramatically in Stage II, indicating a significant

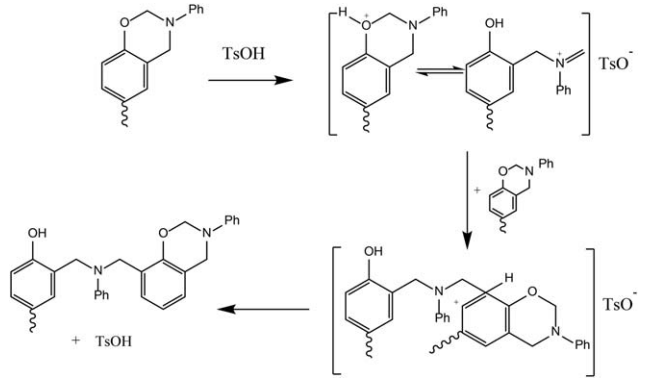


**Figure 1.** Ring opening polymerization of polybenzoxazine catalyzed by *p*-toluenesulfonic acid.[21]

increase in either the population of the particles or the size of the polymer domains due to intramolecular crosslinking.[23] This size increment was later confirmed by the data from DLS measurements. The scattered intensities were monitored until the extracted solutions were found too viscous and could not be diluted any further. Such time was recorded as the gelation time, for example, 51 min in DMSO and 350 min in NMP at 120 °C.

It is evident that the nature of the solvents played an important role in determining the gelation time. It was reported earlier[24] that $pK_a$ of acids in NMP is 1.2 units higher than that in DMSO. In view of this, TSA/DMSO solution produced three to four times higher concentration of $H^+$ than TSA/NMP solution for the same initial concentration of TSA. Accordingly, more BZ monomers underwent initiation and subsequent polymerization in DMSO leading to faster gelation. This is also evident from the significantly higher intensity counts in Figure 2(a) than in Figure 2(b) for a given time.

To further establish a mechanism of PBZ gelation, DLS measurements were used to obtain the average values of $R_h$ as well as the size distribution of the nanoparticles. The CONTIN analysis of DLS data revealed two peaks in Figure 2(c,d) as the PBZ particles grew larger in both solvents. In Figure 2(c,d), $\Gamma G(\Gamma)$ denotes the relative contribution to the total scattered intensity due to particles of a given $R_h$. The main peaks in Figure 2(c,d) are attributed to highly crosslinked polymer particles while the minor ones correspond to oligomers or polymers with relatively low molecular weights. In this regard, in order to simplify the analysis, the following discussion focused on the main peaks with moderate correction of the minor peaks.[25] Figure 2(c,d) presents the size distribution of PBZ in DMSO and NMP at different reaction times. Similar to the trend of scattered intensity from SLS measurements presented in Figure 2(a,b), the $R_h$ of the predominant particles increased slowly initially, followed by a rapid increase. We attribute particle growth in both solvents to *nucleation* and *growth* mechanism. Small particles were observed at the very beginning and their size gradually and slowly increased reminiscent of the nucleation stage. The DLS results indeed nullified the possibility that the networks of strands observed in the case of NMP grew out of spinodal decomposition.

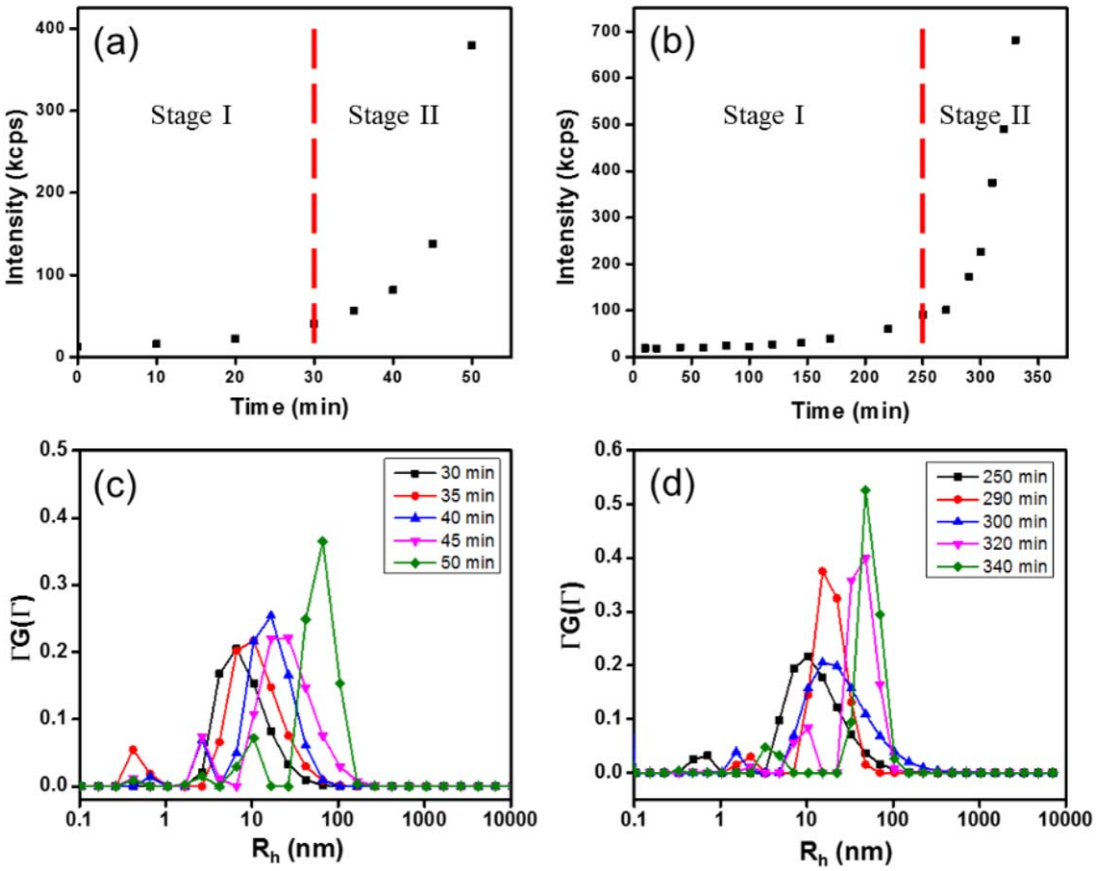


**Figure 2.** Change of total scattered intensities of (a) DMSO solution and (b) NMP solution at 90° angle. CONTIN analysis of DLS studies of (c) DMSO solution and (d) NMP solution at different times. [Color figure can be viewed at wileyonlinelibrary.com]

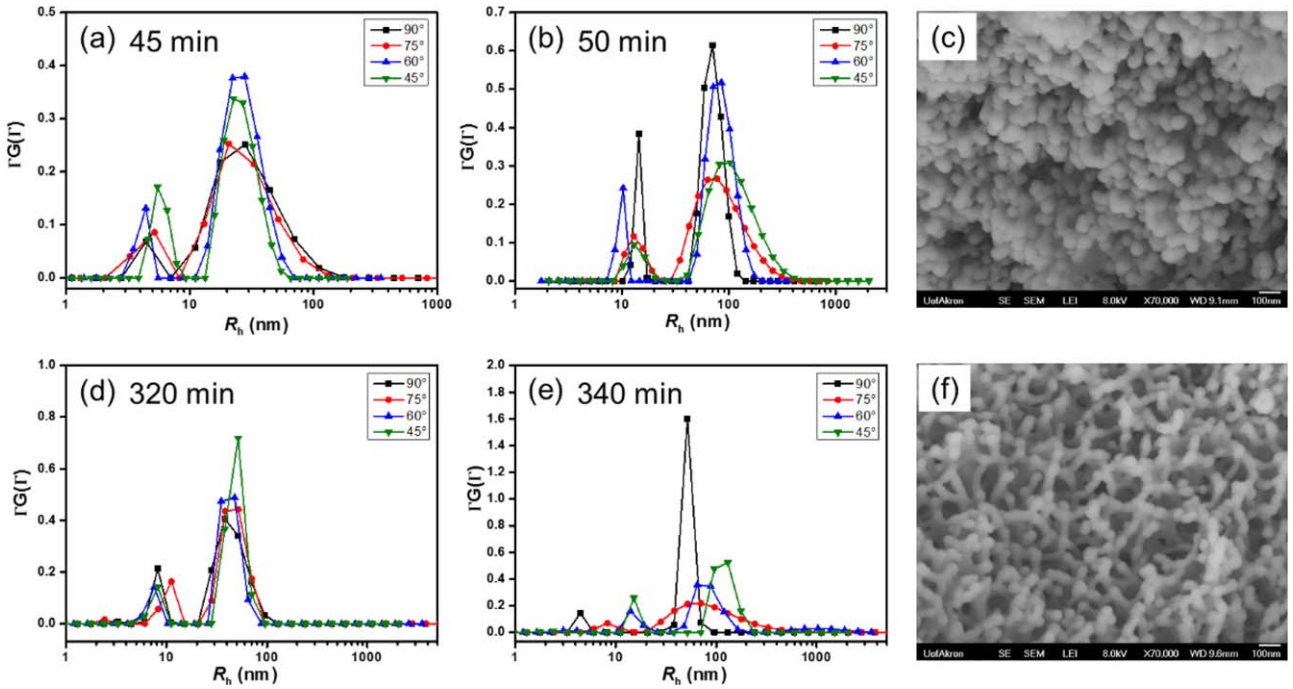


**Figure 3.** At 120 °C, $R_h$ distribution of particles in DMSO after heating for (a) 45 min and (b) 50 min at different scattering angles. (c) SEM image of network of PBZ aerogel synthesized in DMSO. $R_h$ distribution of particles in NMP after heating for (d) 320 min and (e) 340 min at different scattering angles. (f) SEM image of network of PBZ aerogel synthesized in NMP. [Color figure can be viewed at wileyonlinelibrary.com]

**Table I.** $R_h$ and $R_g$ Values of PBZ Nanoparticles Formed in DMSO at 120 °C

| | $R_{h,90°}$ | $R_{h,75°}$ | $R_{h,60°}$ | $R_{h,45°}$ | $R_{h,0°}$ | $R_g$ |
|---|---|---|---|---|---|---|
| 45 min | 21.6 ± 1.0 | 22.5 ± 1.0 | 23.0 ± 1.0 | 19.0 ± 1.0 | 19.5 | —[a] |
| 50 min | 62.0 ± 2.0 | 65.4 ± 2.0 | 77.3 ± 1.5 | 92.4 ± 1.0 | 111.8 | 69.4 ± 1.2 |

Radius unit: nm.
[a] $R_g$ at 45 min is not available as the size was not detectable.

**Table II.** $R_h$ and $R_g$ Values of PBZ Particles Formed in NMP, at 120 °C

| | $R_{h,90°}$ | $R_{h,75°}$ | $R_{h,60°}$ | $R_{h,45°}$ | $R_{h,0°}$ | $R_g$ |
|---|---|---|---|---|---|---|
| 250 min | 10.3 ± 1.0 | 9.9 ± 1.0 | 10.2 ± 1.0 | 10.4 ± 1.2 | 10.3 | —[a] |
| 310 min | 30.7 ± 1.0 | 34.8 ± 1.0 | 34.7 ± 1.1 | 32.8 ± 1.1 | 35.3 | 29.0 ± 0.4 |
| 320 min | 42.6 ± 1.2 | 46.5 ± 1.7 | 40.3 ± 1.2 | 44.9 ± 1.7 | 43.5 | 48.3 ± 0.5 |
| 340 min | 47.1 ± 1.3 | 65.6 ± 1.2 | 72.5 ± 1.5 | 116.9 ± 3.0[b] | 241.7 | 113.1 ± 1.3 |

Radius unit: nm.
[a] $R_g$ at 250 min is not available as the size was not detectable.
[b] Some large PBZ aggregates might have been included.

However, we have not found an answer to the question on how the spheres that formed by nucleation and growth mechanism in NMP led to the strands observed by Gu *et al.*[9] To gain further understanding of the shape of PBZ particles in these solvents, a series of $R_h$ measurements by DLS at different scattering angels and $R_g$ measurements by SLS were performed (Supporting Information Figures S1 and S2). It should be noted that, for solid spheres, $R_h$ at different scattering angles should be almost invariant to the angle of view and $R_g$ should be smaller than $R_h$ at 0° ($R_{h,0}$). In the case of cylindrical particles, however, both angle dependent $R_h$ values and usually, larger $R_g$ values should be observed.[17]

It is apparent from the data presented in Figure 3(a,b) and Table I that in the case of DMSO solution, no obvious difference was observed in values of $R_h$ at different angles, even when the system was close to the gel point. This indicates that PBZ particles were present as single spheres during the polymerization process in DMSO up to a point very close to gelation. At or beyond the gel point, the spheres might have formed random aggregates leading to the PBZ gel network [Figure 3(c)]. The same spherical shape was also observed in the case of NMP solution before the 320 min mark [Figure 3(d), Supporting Information Figure S2]. However, the particles transformed their geometries during the time period between 320 and 340 min [Figure 3(e)]. The $R_h$ values at different scattering angles showed huge differences [Figure 3(d), Table II], and the calculated $R_g$ values are larger or close to the $R_{h,0}$ values, suggesting the formation of anisotropic structures by the joining of two or more spheres. We also conducted PBZ gelation experiments at a lower temperature, for example, at 108 °C, followed by LLS measurements at room temperature (Supporting Information Figures S3–S6). The gelation took relatively longer time, but consistently, the LLS results suggested that the polymer particles also showed the same growth process but lower polymerization rates in both DMSO and NMP solutions (Supporting Information Figures S3–S6).

Based on the evidences gleaned from SLS techniques and SEM images, the mechanism of spherical and cylindrical building block formation of PBZ gels can now be proposed for polymerization in solvents DMSO and NMP. As illustrated in Figure 4, in the first step, tiny polymer nuclei are formed due to polymerization-induced phase separation. The size of the nuclei increases with the molecular weight and the crosslinking density. Such an increase in the particle dimension is referred to as the primary growth regardless of the solvents. In DMSO, nucleation occurs earlier and the particles grow faster due to higher rates of polymerization catalyzed by higher proton concentration. Also, diffusion-limited cluster aggregation[10,25] leads to random packing of the spheres to form the particulate gel networks as seen in Figure 3(c). However, in NMP, the concentration of the initial nuclei is lower at the beginning of the gelation process due to lower rate of polymerization attributed in turn to lower proton concentration. The particles eventually grow larger due to *primary growth*. Meanwhile, the *secondary growth* takes place as the reactive molecules on the surfaces of

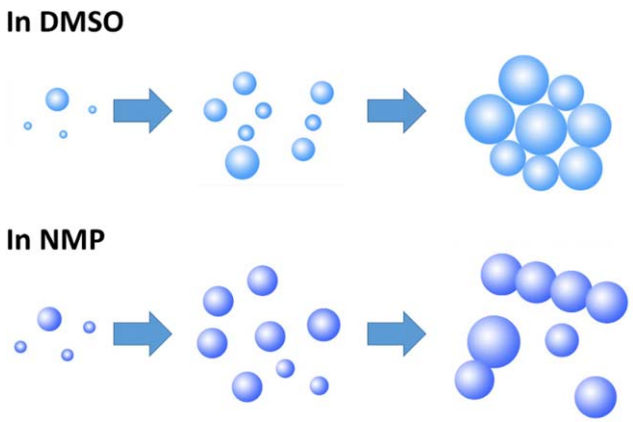


**Figure 4.** Growth models of PBZ gel networks in DMSO and NMP. [Color figure can be viewed at wileyonlinelibrary.com]

different particles connect during interparticle collision. Although the correct mechanism cannot be unequivocally established barring more detailed investigation, we present two possibilities. First, the steric hindrance may account for the end-to-end assembly of the spheres during the *secondary growth*. Another source of secondary growth may be nucleation and growth on the surface of an already formed primary particle. In addition, the size of secondary particles increased with time and the voids between two spheres are partially filled due to concurrent *primary growth*. Eventually, the secondary particles turned into interconnected cylindrical rods as shown in Figures 3(f) and 4. Obtaining convincing experimental evidence of the above scenarios is beyond the scope of the current report.

## CONCLUSIONS

The study showed that LLS technology can be useful in probing the evolution of nanoparticles during phase growth and gelation of PBZ. The analysis of SLS and DLS data confirmed that nucleation and growth was responsible for formation of both spherical and cylindrical building blocks in PBZ gels. The primary growth of spherical particles continued in DMSO until the gel point, while in NMP, the secondary growth occurred via fusion of spheres into cylinders. The method and the observations presented in this letter can be used as a basis for design of microstructures of promising aerogel products.

## REFERENCES


1. Arico, A. S.; Bruce, P.; Scrosati, B.; Tarascon, J.-M.; van Schalkwijk, W. *Nat. Mater.* **2005**, *4*, 366.
2. Horike, S.; Shimomura, S.; Kitagawa, S. *Nat. Chem.* **2009**, *1*, 695.
3. Taguchi, A.; Schüth, F. *Microporous Mesoporous Mater.* **2005**, *77*, 1.
4. Randall, J. P.; Meador, M. A. B.; Jana, S. C. *ACS Appl. Mater Interfaces* **2011**, *3*, 613.
5. Soleimani Dorcheh, A.; Abbasi, M. H. *J. Mater. Process. Technol.* **2008**, *199*, 10.
6. Schmidt, M.; Schwertfeger, F. *J. Non-Cryst. Solids* **1998**, *225*, 364.
7. Kabbour, H.; Baumann, T. F.; Satcher, J. H.; Saulnier, A.; Ahn, C. C. *Chem. Mater.* **2006**, *18*, 6085.
8. Sun, H.; Xu, Z.; Gao, C. *Adv. Mater.* **2013**, *25*, 2632.
9. Gu, S.; Li, Z.; Miyoshi, T.; Jana, S. C. *RSC Adv.* **2680**, *5*, 1.
10. Leventis, N.; Sotiriou-Leventis, C.; Chandrasekaran, N.; Mulik, S.; Larimore, Z. J.; Lu, H.; Churu, G.; Mang, J. T. *Chem. Mater.* **2010**, *22*, 6692.
11. Meador, M. A. B.; Malow, E. J.; Silva, R.; Wright, S.; Quade, D.; Vivod, S. L.; Guo, H.; Guo, J.; Cakmak, M. *ACS Appl. Mater. Interfaces* **2012**, *4*, 536.
12. Pekala, R. W.; Schaefer, D. W. *Macromolecules* **1993**, *26*, 5487.
13. Shinko, A.; Jana, S. C.; Meador, M. A. *RSC Adv.* **2015**, *5*, 105329.
14. Gu, S.; Zhai, C.; Jana, S. C. *Langmuir* **2016**, *32*, 5637.
15. Liu, T. *J. Am. Chem. Soc.* **2003**, *125*, 312.
16. Tanford, C. Physical Chemistry of Macromolecules; Wiley: New York, **1961**.
17. Wang, X.; Qiu, X.; Wu, C. *Macromolecules* **1998**, *31*, 2972.
18. Chu, B. Laser Light Scattering; Academic Press: New York, **1974**.
19. Hiemenz, P. C.; Rajagopalan, R. Principles of Colloid and Surface Chemistry, Revised and Expanded; CRC Press: Boca Raton, FL, **1997**; Vol. *14*.
20. Sudo, A.; Yamashita, H.; Endo, T. *J. Polym. Sci. Part A: Polym. Chem.* **2011**, *49*, 3631.
21. Ning, X.; Ishida, H. *J. Polym. Sci. Part A: Polym. Chem.* **1994**, *32*, 1121.
22. Takeichi, T.; Kano, T.; Agag, T. *Polymer* **2005**, *46*, 12172.
23. Cox, B. G. Acids and Bases: Solvents Effects on Acid-Base Strength; Oxford University Press: Oxford, UK, **2013**.
24. Liu, T.; Rulkens, R.; Wegner, G.; Chu, B. *Macromolecules* **1998**, *31*, 6119.
25. Witten, T. A.; Sander, L. M. *Phys. Rev. Lett.* **1981**, *47*, 1400.